Electronic Journal of Mathematical Analysis and Applications
Vol. 8(2) July 2020, pp. 172-187.
ISSN: 2090-729X(online)
http://math-frac.org/Journals/EJMAA/

SPECTRAL ELEMENT APPROXIMATION OF FUNCTIONAL INTEGRAL EQUATIONS

J. S. AZEVEDO, S. P. OLIVEIRA AND A. M. ROCHA

Abstract. We discuss the existence, uniqueness, and numerical approximation of solutions to a class of nonlinear Fredholm-type integral equations of the second kind. The analysis is performed in the space of square integrable functions, providing the functional setting to study Galerkin approximations. In particular, we choose the spectral element method with Gauss-Lobatto-Legendre collocation points, which leads to an explicit fixed-point problem that is solved with the Picard iterative method. We prove an optimal convergence rate for the proposed iterative method, which is also superconvergent at the quadrature nodes. The theoretical error bounds are verified through numerical experiments as well.

1. Introduction

Nonlinear integral equations have attracted much interest in the last decades, and a vast literature has been devoted to the existence and uniqueness of solutions as well as methods for obtaining exact or approximate solutions [2, 4, 7, 21]. The interest in these equations arises in areas such as physics, engineering, and biology.

In this work, we study the conditions for existence, uniqueness and analyze the convergence of some nonlinear integral equations of Fredholm type known as functional integral equations. These equations take the form

$$u(x) = g(x) + f\left(x, \int_a^b \kappa(x,y)u(y)\,dy\right), \quad x \in [a,b], \tag{1}$$

where $-\infty < a < b < \infty$, f, κ, and g are known functions, and u is the solution to be determined. These equations have found application in the theory of swelling porous media [19]. While previous works on the existence and uniqueness of functional integral equations have been carried out in L^1 spaces [6, 10] and, more recently, in L^∞ spaces [20], we resort to the functional setting of Lebesgue square integrable functions, which is the natural framework for Galerkin methods [4, 5].

We numerically solve equation (1) with the spectral element method (SEM), a high-order Galerkin method that combines the accuracy of spectral methods with

2010 *Mathematics Subject Classification.* 45D05, 45G10, 46E35, 65R20.
Key words and phrases. Nonlinear Fredholm Integral Equations, Spectral Element Method, Picard Iteration.
Submitted Dec. 12, 2019. Revised Dec. 17, 2019.

the flexibility of finite elements [17]. Oliveira and Azevedo [15] computed the SEM solution to homogeneous Fredholm integral equations of second kind incorporating Gauss-Lobatto-Legendre (GLL) collocation points. Zakian and Khaji [23] also used SEM with GLL points to perform the Karhunen-Loève expansion of covariance functions; the same spectral element basis was employed in the spatial discretization of the elastic wave equation with random coefficients. It is worth noting that other high-order numerical methods, such as wavelets [12, 16, 18] and spectral Galerkin methods [1, 22], have also been applied to integral equations. High-order convergence may also be achieved through iterated Galerkin methods [14].

The SEM discretization of equation (1) results in a system of non-linear equations that are solved by the Picard iterative method, as in [20]. We perform a convergence analysis of the fully-discrete scheme, proving that the error in the L^2-norm is of order up to $\mathcal{O}(h^{N+1})$, where N is the polynomial degree of the spectral elements. Moreover, if the error is measured with the GLL quadrature, then the order can be as high as $\mathcal{O}(h^{2N})$. As illustrated by the numerical examples, such estimates strongly depend on the regularity of the input data.

2. Preliminary assumptions

The functional setting for this work is the Hilbert space $L^2([a,b])$ defined with the usual inner product and induced norm

$$\langle u, v\rangle = \int_a^b u(x)v(x)\,dx, \quad \|v\|_0 = \langle v, v\rangle^{1/2}, \tag{2}$$

along with the spaces $H^m([a,b]) = \{v : \frac{\partial^k v}{\partial x^k} \in L^2([a,b]),\ 0 \le k \le m,\ m \ge 1\}$ equipped with the norms

$$\|v\|_m = \left(\sum_{k=0}^{m} |v|_m^2\right)^{\frac{1}{2}}, \quad |v|_m = \left\|\frac{\partial^k v}{\partial x^k}\right\|_0. \tag{3}$$

For convenience, we denote the standard norm in $L^2([a,b]^2)$ also as $\|\cdot\|_0$.

In order to rewrite the functional integral equation (1) in operator form, let K be the integral linear operator given by

$$(Ku)(x) = \int_a^b \kappa(x,y)u(y)\,dy, \tag{4}$$

let F be the superposition operator defined by $(Fu)(x) = f(x, u(x))$, and let $G = FK$, i.e,

$$(Gu)(x) = (FKu)(x) = f\left(x, \int_a^b \kappa(x,y)u(y)\,dy\right). \tag{5}$$

We have that equation (1) reduces to the fixed-point equation $u = Au$, where

$$Au = g + Gu. \tag{6}$$

We will see below that the results of existence and uniqueness are based in determining a fixed point for the operator A. To this end, we will consider the following conditions on the functions g, f and κ:

Assumption 2.1.
(A1) $g \in L^2([a,b])$;
(A2) $\kappa \in L^2([a,b]^2)$;

(A3) *$f : [a,b] \times \mathbb{R} \longrightarrow \mathbb{R}$ satisfies the Carathéodory's conditions and there is a positive constant $\tau_1 > 0$ and a nonnegative function $\theta_1 \in L^2([a,b])$ such that*

$$|f(x,y)| \leq \theta_1(x) + \tau_1|y|, \quad y \in \mathbb{R},\ x \in [a,b].$$

(A4) *f is Lipschitz with respect to the second variable with Lipschitz constant $\tau_2 > 0$, i.e.,*

$$|f(x,u) - f(x,v)| \leq \tau_2|u-v|, \quad x \in [a,b],\ u,v \in \mathbb{R}.$$

(A5) *the kernel κ and the constant τ_2 satisfy $\tau_2\|\kappa\|_0 < 1$.*

3. Existence and uniqueness on $L^2([a,b])$

We begin with a preliminary result showing that A maps $L^2([a,b])$ into $L^2([a,b])$.

Lemma 3.1. *$Au \in L^2([a,b])$ for any $u \in L^2([a,b])$.*

Proof. It suffices to show that the operator G maps $L^2([a,b])$ into $L^2([a,b])$. Given $u \in L^2([a,b])$, using the inequality in *(A3)* we have

$$\|Gu\|_0 \leq \left(\int_a^b |\theta_1(x) + \tau_1 |(Ku)(x)||^2\ dx\right)^{1/2}.$$

Applying Minkowski's inequality, we find

$$\begin{aligned}\|Gu\|_0 &\leq \left(\int_a^b |\theta_1(x)|^2\ dx\right)^{1/2} + \left(\int_a^b |\tau_1 |(Ku)(x)||^2\ dx\right)^{1/2} \\ &= \|\theta_1\|_0 + \tau_1 \left(\int_a^b \left|\int_a^b \kappa(x,y)u(y)\,dy\right|^2 dx\right)^{1/2},\end{aligned}$$

Afterwards, it follows from Hölder's inequality that

$$\begin{aligned}\|Gu\|_0 &\leq \|\theta_1\|_0 + \tau_1 \left\{\int_a^b \left[\left(\int_a^b |\kappa(x,y)|^2\,dy\right)^{1/2}\left(\int_a^b |u(y)|^2\,dy\right)^{1/2}\right]^2 dx\right\}^{1/2} \\ &= \|\theta_1\|_0 + \tau_1 \left(\int_a^b\int_a^b |\kappa(x,y)|^2\,dy\,dx\right)^{1/2} \|u\|_0 \\ &= \|\theta_1\|_0 + \tau_1\|\kappa\|_0\,\|u\|_0,\end{aligned}$$

which implies that $Gu \in L^2([a,b])$. □

Theorem 3.1. *There exists a unique function $u \in L^2([a,b])$ such that $u = Au$.*

Proof. We have from Lemma 3.1 that A maps $L^2([a,b])$ to $L^2([a,b])$. From the Banach Fixed Point Theorem, it remains to prove that A is a contraction. Indeed, we have from *(A4)* that

$$\|Au - Av\|_0 \leq \tau_2\|Ku - Kv\|_0 \leq \tau_2\|K\|_0\|u-v\|_0, \quad \|K\|_0 = \sup_{\|u\|_0=1} \|Ku\|_0.$$

Using Hölder's inequality as in Lemma 3.1, we find $\|K\|_0 \leq \|\kappa\|_0$, thus $\|Au - Av\|_0 \leq \tau_2\|\kappa\|_0\|u-v\|_0$, and the contraction follows from condition *(A5)*. □

4. Spectral element approximation

For the purpose of finding an approximate solution to (1), we construct a finite-dimensional space $V_h = \text{span}\{\phi_1, \phi_2, \ldots, \phi_n\} \subset L^2([a,b])$ and seek the Galerkin approximation $u_h \in V_h$ such that

$$\langle u_h, v_h\rangle = \langle g, v_h\rangle + \langle Gu_h, v_h\rangle, \quad \forall\ v_h \in V_h. \tag{7}$$

The basis functions ϕ_I $(1 \le I \le n)$ are Lagrange piecewise polynomial functions of degree N satisfying the relation $\phi_I(x_J) = \delta_{I,J}$, where x_J are the spectral element nodes defined as follows. We partition the interval $[a,b]$ into N_e elements with uniform spacing $h := (b-a)/N_e$, and subdivided into N interior intervals, leading to a total of $n = N_eN+1$ nodes. For any element index $1 \le e \le N_e$ and local index $0 \le j \le N$, the global nodal index is $IEN(j,e) = j + (e-1)N + 1$. The global nodes are $x_J = F^e(\xi_j)$, where $J = IEN(j,e)$, F^e is the linear transformation from $[-1,1]$ to the e-th element, and ξ_j is the j-th GLL collocation point.

The main motivation for choosing GLL points in the SEM is that the global nodes provide the following compound Gauss-Lobatto quadrature:

$$\int_a^b f(x)\,dx \approx \sum_{e=1}^{N_e}\sum_{j=0}^{N} \hat{w}_j f(F^e(\xi_j))J^e = \sum_{J=1}^{n} w_J f(x_J), \tag{8}$$

which is exact for piecewise polynomials of degree $2N-1$ [8]. Here J^e represents the determinant of the Jacobian matrix of the transformation F^e. The global weights w_J are

$$w_J = \sum_{(j,e)\in IEN_J} \hat{w}_j J^e, \quad IEN_J = \{(j,e)\,;J = IEN(j,e)\}. \tag{9}$$

When we apply quadrature (8) to the Galerkin approximation (7), we obtain a collocation-type scheme that is simpler than standard Galerkin discrete systems. Indeed, let us write the Galerkin solution as

$$u_h(x) = \sum_{J=1}^{n} u_J\phi_J(x). \tag{10}$$

By choosing $v_h = \phi_I$, $1 \le I \le n$, we find

$$\begin{aligned}\sum_{J=1}^{n} u_J \int_a^b \phi_J(x)\phi_I(x)\,dx &= \int_a^b g(x)\phi_I(x)\,dx \\ &+ \int_a^b f\left(x, \sum_{J=1}^{n} u_J\left(K\phi_J\right)(x)\right)\phi_I(x)\,dx, \quad I = 1,\ldots,n,\end{aligned} \tag{11}$$

Employing the quadrature (8) and recalling that $\phi_I(x_J) = \delta_{I,J}$, it follows that the system of equations (11) reduces to the following explicit scheme:

$$u_I = g(x_I) + f\left(x_I, \sum_{J=1}^{n} u_J w_J \kappa(x_I, x_J)\right), \quad I = 1,\ldots,n. \tag{12}$$

4.1. **Iterative process.** Let $\boldsymbol{u} = [u_1,\ldots,u_n]^T$ be the vector of coefficients of the Galerkin solution (10). We can rewrite (12) in vector form as

$$\boldsymbol{u} = \boldsymbol{A}(\boldsymbol{u}), \quad \boldsymbol{A}(\boldsymbol{u}) = \boldsymbol{g} + \boldsymbol{F}(\boldsymbol{K}\boldsymbol{u}), \tag{13}$$

with

$$\begin{cases} F_I(\boldsymbol{y}) = f(x_I, y_I), \\ g_I = g(x_I). \\ K_{I,J} = w_J \kappa(x_I, x_J), \qquad 1 \leq I, J \leq n. \end{cases} \tag{14}$$

Through Picard iteration, the nonlinear algebraic system (13) is approximated as follows:

$$\boldsymbol{u}^{(k+1)} = \boldsymbol{A}(\boldsymbol{u}^{(k)}), \quad k = 0, 1, 2, \ldots, \tag{15}$$

where $\boldsymbol{u}^{(k)} = [u_1^{(k)}, \ldots, u_n^{(k)}]^T$.

5. Convergence Analysis

In the following we prove that the approximate solution obtained by the iterative scheme (15) converges to the solution of (1) under the same assumptions of Theorem 3.1 and additional regularity hypotheses.

Since the approximate solution $\mathbf{u}^{(k)} = [u_1^{(k)}, \ldots, u_n^{(k)}]^T$ from (15) and the exact solution u are not in the same vector space, we consider the function $u_h^{(k)} \in V_h$ given by expression

$$u_h^{(k)}(x) = \sum_{J=1}^{n} u_J^{(k)} \phi_J(x). \tag{16}$$

Defining the global error as

$$e_{h,k} = \|u - u_h^{(k)}\|_0, \tag{17}$$

we can estimate it by the following expression:

$$e_{h,k} \leq \|u - u_h\|_0 + \|u_h - u_h^{(k)}\|_0, \tag{18}$$

where u_h is the exact solution of (12).

Let us separately analyze each term of expression (18). The first term represents the error of the spectral element method, while the second term takes into account the error of the Picard iteration.

5.1. Convergence of the spectral element method.

We start reviewing some approximation theory results that are important to the error analysis. From here on, C denotes a generic positive constant that does not depend on the element length h.

Lemma 5.1. *(see* [9, Theorem 3.2.1]*) The interpolation operator*

$$I_h v(x) = \sum_{J=1}^{n} v(x_J) \phi_J(x) \tag{19}$$

satisfies the following estimate for any $v \in H^s([a,b])$ with $s \leq N+1$:

$$\|v - I_h v\|_0 \leq C h^s |v|_s. \tag{20}$$

Lemma 5.2. *Let $u, v \in H^k([a,b])$ with $k \leq 2N$. There holds*

$$|\langle u, v \rangle - \langle u, v \rangle_h| \leq C h^k |u|_k |v|_k, \tag{21}$$

where $\langle \cdot, \cdot \rangle_h$ denotes the discrete inner product

$$\langle u, v \rangle_h = \sum_{J=1}^{n} w_J u(x_J) v(x_J). \tag{22}$$

In particular, we have

$$\left|\|u\|^2 - \|u\|_h^2\right| \leq Ch^k |u|_k^2, \tag{23}$$

where $\|v\|_h = \sqrt{\langle v, v\rangle_h}$. *Moreover, the two-dimensional counterpart of* (23) *also holds if* $u \in H^k([a,b]^2)$.

Proof. Recalling that the GLL quadrature is exact for piecewise polynomials of degree $2N-1$, the above error estimates can be verified at each element through Bramble-Hilbert Lemma, as in [3, Theorem 3.5]. □

Lemma 5.3. *(see* [3, Lemma 3.2]*) The norm* $\|\cdot\|_0$ *is equivalent to* $\|\cdot\|_h$ *in space* V_h, *i.e., there exist* $C_1, C_2 > 0$ *such that*

$$C_1\|v_h\|_0^2 \leq \|v_h\|_h^2 \leq C_2\|v_h\|_0^2 \quad \forall v_h \in V_h. \tag{24}$$

Next we prove the theorem that provides an error estimate for the first term of expression (18):

Theorem 5.1. *Let* u *be the exact solution of equation* (1) *and let* u_h *be the solution of the nonlinear system* (12). *If* $f : [a,b] \times \mathbb{R} \longrightarrow \mathbb{R}$ *satisfies Part (A4) of Assumption 2.1,* $\kappa \in H^p([a,b]^2)$, *and* $u \in H^p([a,b])$ *with* $p \leq 2N$, *then there exists* $h_0 > 0$ *such that, for* $h \leq h_0$,

$$\|u - u_h\|_h \leq Ch^p |u|_p, \tag{25}$$

$$\|u - u_h\|_0 \leq Ch^s |u|_s, \quad s = \min(p, N+1). \tag{26}$$

Proof. The proof is structured similarly as in Theorem 4.1 in [22]. We have from (1) and (12) that

$$u(x_I) - u_I = S_I, \quad S_I = f\left(x_I, \langle \kappa(x_I, \cdot), u\rangle\right) - f\left(x_I, \langle \kappa(x_I, \cdot), u_h\rangle_h\right), \tag{27}$$

for $1 \leq I \leq n$. Note from (27) that

$$\|u - u_h\|_h = \left(\sum_{I=1}^{n} w_I |S_I|^2\right)^{1/2}. \tag{28}$$

We must find an upper bound for the right-hand side of (28). We have from Lemma 5.2 and condition *(A4)* that

$$\begin{aligned}
|S_I| &\leq \tau_2 \left|\langle \kappa(x_I, \cdot), u\rangle - \langle \kappa(x_I, \cdot), u_h\rangle_h\right| \\
&\leq \tau_2 \left|\langle \kappa(x_I, \cdot), u\rangle - \langle \kappa(x_I, \cdot), u\rangle_h\right| + \tau_2 \left|\langle \kappa(x_I, \cdot), u\rangle_h - \langle \kappa(x_I, \cdot), u_h\rangle_h\right| \\
&\leq Ch^p |\kappa(x_I, \cdot)|_p |u|_p + \tau_2 \left|\sum_{J=1}^{n} w_J \kappa(x_I, x_J)[u(x_J) - u_J]\right| \\
&\leq \tau_2 \left(\sum_{J=1}^{n} w_J \left|\kappa(x_I, x_J)\right|^2 \sum_{J=1}^{n} w_J \left|u(x_J) - u_J\right|^2\right)^{1/2} + Ch^p |\kappa(x_I, \cdot)|_p |u|_p, \\
&= \tau_2 \|u - u_h\|_h \left(\sum_{J=1}^{n} w_J \left|\kappa(x_I, x_J)\right|^2\right)^{1/2} + Ch^p |\kappa(x_I, \cdot)|_p |u|_p.
\end{aligned}$$

It follows from Minkowski's inequality that

$$\left(\sum_{I=1}^{n} w_I|S_I|^2\right)^{1/2} \leq \tau_2\|u-u_h\|_h \left(\sum_{I,J=1}^{n} w_I w_J \left|\kappa(x_I,x_J)\right|^2\right)^{1/2} + Ch^p|u|_p \left(\sum_{I=1}^{n} w_I|\kappa(x_I,\cdot)|_p^2\right)^{1/2},$$

and using again Lemma 5.2, we have that there exists $\tilde{C}>0$ such that

$$\begin{aligned}\left(\sum_{I=1}^{n} w_I|S_I|^2\right)^{1/2} &\leq \tau_2\|u-u_h\|_h \left(\|\kappa\|_0 + \tilde{C}h^{p/2}|\kappa|_p\right) \\ &\quad + Ch^p|u|_p \left(\left\|\frac{\partial^p\kappa}{\partial y^p}\right\|_0 + \tilde{C}h^{p/2}|\kappa|_p\right).\end{aligned} \tag{29}$$

Thus, there exists a constant C depending on κ such that

$$\left(1-\tau_2\|\kappa\|_0 - \tau_2\tilde{C}h^p|\kappa|_p\right)\|u-u_h\|_h \leq Ch^p|u|_p, \tag{30}$$

and estimate (25) follows from part *(A5)* if $h \leq h_0$, where h_0 is such that $0 < \tau_2\tilde{C}h_0^p|\kappa|_p < 1-\tau_2\|\kappa\|_0$. On the other hand, let $s=\min(p,N+1)$. It follows from the triangular inequality and Lemmas 5.1 and 5.3 that

$$\|u-u_h\|_0 \leq \|u-I_hu\|_0 + \|I_hu-u_h\|_0 \leq Ch^s|u|_s + C_2\|I_hu-u_h\|_h. \tag{31}$$

Noting that $\|I_hu-u_h\|_h = \|u-u_h\|_h$, (26) follows from (31) and (25). □

5.2. **Convergence of Picard Iteration.** In the following we study the error in matrix formulation (13) due to the iterative process (15). For this purpose, we introduce the following vector norm associated with the GLL quadrature:

$$\|\boldsymbol{v}\|_w^2 = \sum_{I=1}^{n} w_I|v_I|^2. \tag{32}$$

Theorem 5.2. *Under Assumption 2.1 the operator* $\boldsymbol{A}: \mathbb{R}^n \longrightarrow \mathbb{R}^n$, *defined by*

$$\boldsymbol{A}(\boldsymbol{u}) = \boldsymbol{g} + \boldsymbol{F}(\boldsymbol{K}\boldsymbol{u}). \tag{33}$$

is a contraction with respect to the norm $\|\cdot\|_w$.

Proof. By definition of the operator $\mathbf{A}$ and norm $\|\cdot\|_w$, we have

$$\|\boldsymbol{A}(\boldsymbol{u})-\boldsymbol{A}(\mathbf{v})\|_w^2 = \sum_{I=1}^{n} w_I \left| f\left(x_I, \sum_{J=1}^{n} w_J\kappa(x_I,x_J)u_J\right) - f\left(x_I, \sum_{J=1}^{n} w_J\kappa(x_I,x_J)v_J\right)\right|^2.$$

Using the condition *(A4)*, Hölder's inequality, and Lemma 5.2, it follows that

$$\begin{aligned}
\|\boldsymbol{A}(\boldsymbol{u}) - \boldsymbol{A}(\boldsymbol{v})\|_w^2 &\leq \tau_2^2 \sum_{I=1}^{n} w_I \left| \sum_{J=1}^{n} w_J \kappa(x_I, x_J)(u_J - v_J) \right|^2 \\
&\leq \tau_2^2 \sum_{I=1}^{n} w_I \left(\sum_{J=1}^{n} w_J \left|\kappa(x_I, x_J)\right|^2 \right) \left(\sum_{J=1}^{n} w_J |u_J - v_J|^2 \right) \\
&= \tau_2^2 \left(\sum_{I,J=1}^{n} w_I w_J |\kappa(x_I, x_J)|^2 \right) \|\boldsymbol{u} - \boldsymbol{v}\|_w^2. \\
&= M\|\boldsymbol{u} - \boldsymbol{v}\|_w^2,
\end{aligned}$$

where

$$M = \tau_2^2 \left(\|\kappa\|_0^2 + Ch^{p/2} |\kappa|_p \right). \tag{34}$$

By taking h sufficiently small and recalling from *(A5)* that $\tau_2 \|\kappa\|_0 < 1$, we have $M < 1$, i.e., $\mathbf{A}$ is a contraction. □

Corollary 5.3. *The sequence* $\{u_h^{(k)}\}_k$ *defined in* (16) *converges to the solution* u_h *of* (7) *for any initial guess* $u_h^{(0)}$. *Moreover,*

$$\|u_h - u_h^{(k)}\|_0 \leq C \frac{M^k}{1 - M} r_0, \quad r_0 = \|A u_h^{(0)} - u_h^{(0)}\|_0, \tag{35}$$

where M *is given by* (34).

Proof. We have from Banach Fixed Point Theorem that the sequence $\{\boldsymbol{u}^{(k)}\}_{k \in \mathbb{N}}$ generated by Picard iteration (15) converges to $\boldsymbol{u}$ in (13) for any $k \geq k_0$ and any initial guess $\boldsymbol{u}^{(0)}$. Moreover,

$$\|\boldsymbol{u} - \boldsymbol{u}^{(k)}\|_w \leq \frac{M^k}{1 - M} \|A\boldsymbol{u}^{(0)} - \boldsymbol{u}^{(0)}\|_w. \tag{36}$$

Noting that $\|v_h\|_h = \|\boldsymbol{v}\|_w$ if $\boldsymbol{v} = [v_1, \ldots, v_n]^T$ and v_h are such that

$$v_h(x) = \sum_{I=1}^{n} v_I \phi_I(x),$$

the proof follows from Lemma 5.3. □

5.3. **Global convergence of the error.** We are now ready to state the main result of this section:

Theorem 5.4. *Let Assumption 2.1 hold and assume* $u \in H^p([a, b])$ *(*$1 \leq p \leq N+1$*) is the solution to* (1). *There is* $h_0 > 0$ *such that for any* $h \leq h_0$, *there exists* $k(h) > 0$ *for which the total error* $e_{h,k}$ *defined in* (17) *satisfies*

$$e_{h,k} \leq Ch^p |u|_p, \quad k \geq k(h). \tag{37}$$

Proof. Choosing $k(h) \leq p \log_M h$, inequality (37) follows from (18), (26), and (35). □

Remark 5.1. *Analogously to Theorem 5.4, if* $u \in H^p([a, b])$ *with* $1 \leq p \leq 2N$, *then* $\|u - u_h^{(k)}\|_h \leq Ch^p |u|_p$ *for* k *sufficiently large.*

6. Numerical experiments

In this section, we provide examples that illustrate the proposed theory. We employ the following stopping criteria:

$$k \leq k_{max},\ r_k = \|\boldsymbol{u}^{(k)} - \boldsymbol{u}^{(k-1)}\|_w > tol_1,\ \|\boldsymbol{u}^{(k-1)}\|_w < tol_2, \tag{38}$$

with $k_{max} = 1000$, $tol_1 = 10^{-15}$, and $tol_2 = 10\|\boldsymbol{u}^{(0)}\|_w$. In order to allow comparing the results across the examples, the error was computed using the following relative measures:

$$e_k = \frac{e_{h,k}}{\|u\|_0} = \frac{\|u - u_h^{(k)}\|_0}{\|u\|_0}, \quad E_k = \frac{\|u - u_h^{(k)}\|_h}{\|u\|_h}. \tag{39}$$

We approximate $\|\cdot\|_0$ by the GLL quadrature of degree 12 with 512 elements. In all experiments, we take as initial guess the constant function $u_h^{(0)}(x) = 2$.

6.1. **Example 1.** Let us consider the functional integral equation (1) with $[a, b] = [0, \pi]$, $\kappa(x, y) = \sin(y - x)$, and $f(x, y) = \cos(y)$. The function g is chosen such that the exact solution is $u(x) = \exp(x)$, i.e.,

$$g(x) = e^x - \cos\left(\frac{\sin(x) + \cos(x)}{2}(e^\pi + 1)\right). \tag{40}$$

Note that the exact solution u, and the kernel κ are infinitely differentiable, in accordance with the conditions of Theorem 5.4. In order to compare the proposed method with better known techniques, we include in this example the collocation method with piecewise linear basis functions [5, 20].

In the following, we study the dependence of the error on the mesh refinement h and the polynomial degree N. As shown in Fig. 1, the relative errors e_k and E_k decay with order $O(h^{N+1})$ and $O(h^{2N})$, respectively, as indicated by the slopes of the linear regression lines. The numerical results appear to be in good agreement with the theoretical result obtained in Theorem 5.4. The only exception is the relative error E_k for $N = 4$, where the error tolerance tol_1 is rapidly reached in the Picard iterations. The relative errors e_k and E_k of the collocation method (Coll) are nearly identical to the GLL method with $N = 1$. Because a similar behavior has been also observed in the next examples, we will not present the error curves for Coll in the remainder of this section.

6.2. **Example 2.** In this example we investigate the parameter-dependent integral equation

$$\begin{aligned} u(x) \;=\; & \frac{1}{100}\cos^2(x) + \left(\frac{2}{100} + \frac{1+\lambda^2}{2\lambda}\right)\cos(x) - \left(\frac{\lambda}{2} + \frac{1}{100}\right) \\ & + \frac{1}{100}\left(\int_0^{4\pi} e^{-\lambda|x-y|}u(y)\,dy\right)^2, \quad x \in [0, 4\pi], \end{aligned} \tag{41}$$

which has been studied in [20], and has the following exact solution:

$$u(x) = \frac{1}{2\lambda}\left[(1+\lambda^2)\cos(x) - \lambda^2\right]. \tag{42}$$

Note that the kernel $\kappa(x, y) = e^{-\lambda|x-y|}$ is not differentiable at $x = y$, whereas $f(x, y) = y^2/100$ is not a Lipschitz function in second variable, thus the conditions of Assumption 2.1 are not fully met.

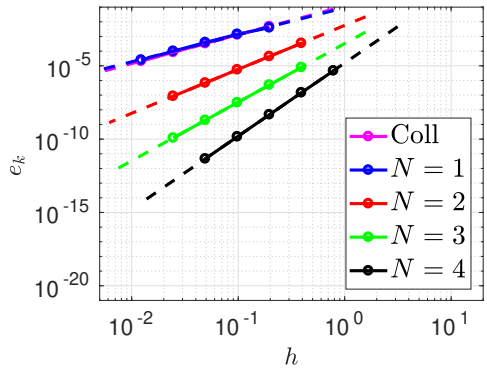

(a)

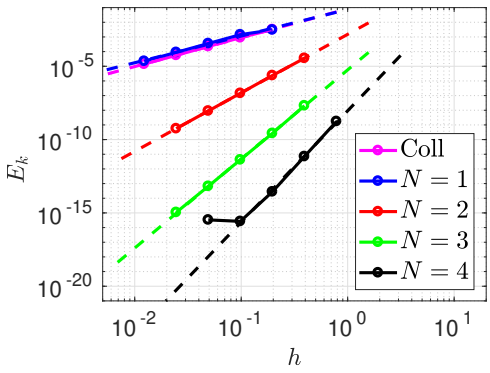

(b)

FIGURE 1. Relative errors e_k (a) and E_k (b) in Example 6.1. The slopes of the dashed lines for e_k are 2.0 (Coll), 1.9 ($N = 1$), 3.0 ($N = 2$), 4.0 ($N = 3$) and 5.0 ($N = 4$), while those for E_k are 2.0 (Coll), 1.8 ($N = 1$), 4.0 ($N = 2$), 6.0 ($N = 3$) and 7.6 ($N = 4$).

The influence of the parameters λ in the approximation error is illustrated in Figure 2. The dependence on parameter λ can be explained from the fact that the exact solution (42) behaves as a constant function (hence easier to approximate) when either $\lambda \to 0$ or $\lambda \to \infty$.

In Figure 3 we choose the parameter $\lambda = 10$ and numerically evaluate the convergence rate in terms of the element length h, as in Figure 1. The convergence rates of the relative errors e_k and E_k are $\mathcal{O}(h^2)$ regardless of the degree N (though the errors consistently decrease with N), due to discontinuity of the first derivative of $\kappa(x, y)$ when $x = y$. In general, as implied by Theorem 5.1, the smoothness of the kernel κ strongly influences the convergence rate of the method.

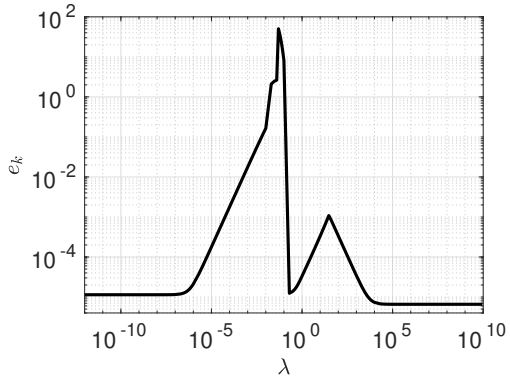

FIGURE 2. Variation of the relative error e_k with respect to parameter λ in Example 6.2 with $N_e = 100$ and $N = 2$.

6.3. **Example 3.** We consider next a problem for which the exact solution is not known. Here, $[a, b] = [0, \pi]$ and $\kappa(x, y)$ is a Gaussian kernel written as

$$\kappa(x, y) = e^{-\lambda^2 (x-y)^2},$$

where the parameter λ defines the length scale, while $f(x, y) = \sin(y)$ and $g(x) = \sqrt{x^2 + x + 2}$. A reference solution is calculated with the GLL spectral element method of degree $N = 12$ using $N_e = 512$ elements.

Firstly, we study how the parameter λ affects the error. Fig. 4 shows the dependence of the relative error e_k on the parameter λ. Clearly, a large value of λ (equivalent to a small amount of smoothing) favors a large error, while a small λ (i.e., a large amount of smoothing) stabilizes error at a small value. We infer from the results of Example 6.2 that the exact solution depends on the length scale λ as in (42), and it might behave as a constant function as $\lambda \to 0$.

We proceed to the numerical convergence analysis of relative errors e_k and E_k for $\lambda = 1$, summarized by Figures 5(a) and 5(b) respectively. As expected, the experiments suggest an order of convergence $\mathcal{O}(h^{N+1})$ in norm $\|\cdot\|_0$ and $\mathcal{O}(h^{2N})$ in norm $\|\cdot\|_h$, validating our theoretical results.

6.4. **Example 4.** The last example aims to verify the applicability of the proposed method to two-dimensional functional integral equations. For this purpose, we consider the following equation, adapted from [13]:

$$u(x, y) = g(x, y) + \sin\left(\int_0^1 \int_0^1 \frac{x}{(8 + y)(1 + t + s)} u(t, s)\, dtds\right), \tag{43}$$

where $(x, y) \in [0, 1] \times [0, 1]$ and

$$g(x, y) = \frac{1}{(1 + x + y)^2} - \sin\left(\frac{x}{6(8 + y)}\right).$$

A exact solution is given by

$$u(x, y) = \frac{1}{(1 + x + y)^2}.$$

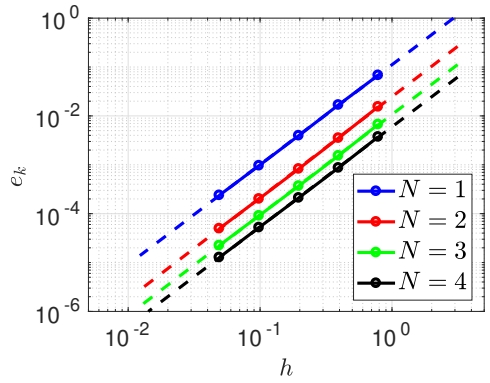

(a)

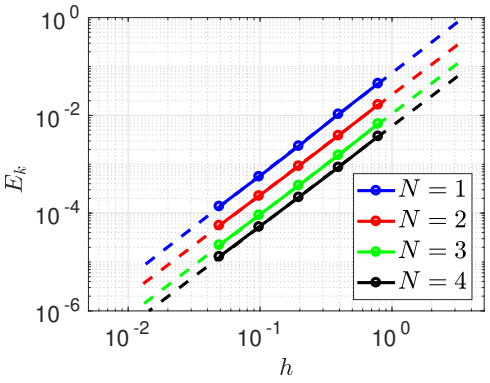

(b)

FIGURE 3. Relative errors e_k (a) and E_k (b) in Example 6.2, with $\lambda = 10$. The slopes of the dashed lines for both e_k and E_k are nearly equal to 2.0.

As in [15], we employ a two-dimensional spectral element approximation over a square grid based on a tensor-product extension of the one-dimensional method described in Sec. 4. The relative errors E_k of Example 6.4 are shown in Fig. 6, and their convergence rates are the same as in the numerical and theoretical results in one dimension.

7. Conclusions

This paper proposes the use of spectral element methods for functional integral equations of the form (1). We have proven conditions of existence and uniqueness in L^2-norm under Assumption 2.1 above, which complement previous works that consider the L^1-norm [6, 10, 11] and the L^∞-norm [20].

For the numerical approximation, we have been able to demonstrate that the global error has optimal order $O(h^{N+1})$ in the L^2 norm $\|\cdot\|_0$ (the same order as the interpolant of the exact solution) and is superconvergent in $\|\cdot\|_0$, with convergence

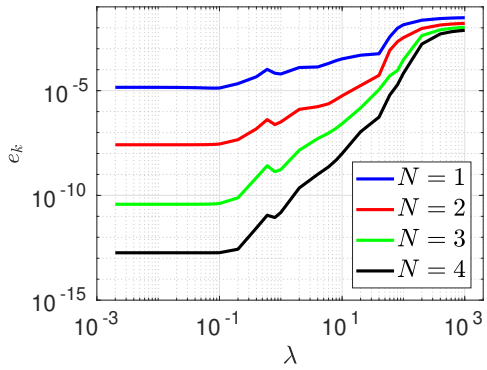

FIGURE 4. Relative error e_k of Example 6.3 in terms of the parameter λ, with $N_e = 100$.

rate $O(h^{2N})$ (the same order of the quadrature error), provided that the hypotheses of Theorem 5.4 hold and the input data are sufficiently regular. It should be noted that convergence assumptions are easy to verify and are useful for selecting the spectral element discretization (for instance, the polynomial degree should not be high if the kernel is not smooth, as illustrated by Example 6.2). The theoretical results have been confirmed by one-dimensional numerical experiments, but can also be extended to higher dimensions, as suggested by Example 6.4.

We expect that the techniques employed herein to analyze functional integral equations can be useful in the study of more classes of nonlinear integral equations, as well as that the spectral element method can be an attractive alternative to more traditional high-order methods for integral equations.

8. Acknowledgements

S. P. Oliveira is supported by CNPq under the grant 313100/2017-9.

References

[1] C. Allouch, D. Sbibih, and M. Tahrichi. Legendre superconvergent Galerkin-collocation type methods for Hammerstein equations. *J. Comput. Appl. Math*, 353:253–264, 2019.

[2] D. G. Anderson. Iterative procedures for nonlinear integral equations. *Journal of the ACM*, 12(4):547–560, 1965.

[3] A. Andreev, V. Kascieva, and M. Vanmaele. Some results in lumped mass finite-element approximation of eigenvalue problems using numerical quadrature formulas. *J. Comput. Appl. Math.*, 43(3):291–311, 1992.

[4] K. E. Atkinson. A survey of numerical methods for solving nonlinear integral equations. *J. Integral Equations Appl.*, 4(1):15–46, 1992.

[5] K. E. Atkinson and J. Flores. The discrete collocation method for nonlinear integral equations. *IMA J. Numer. Anal.*, 13(2):195–213, 1993.

[6] J. Banaś and Z. Knap. Integrable solutions of a functional-integral equation. *Rev. Mat. Univ. Complut.*, 2(1):31–38, 1989.

[7] I. Boglaev. A numerical method for solving nonlinear integro-differential equations of Fredholm type. *J. Comput. Math.*, 34(3), 2016.

[8] C. Canuto, M. Hussaini, A. Quarteroni, and T. Zang. *Spectral Methods: Fundamentals in Single Domains*. Springer-Verlag, New York, 2006.

[9] P. Ciarlet. *The Finite Element Method for Elliptic Problems*. SIAM, Philadelphia, 2002.

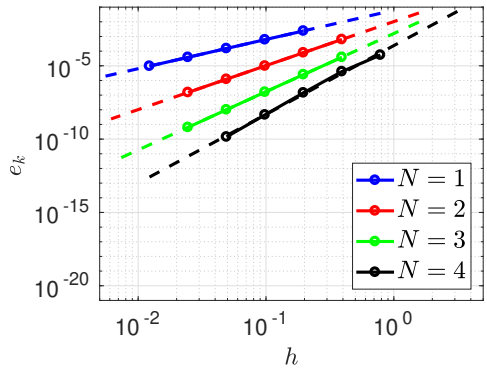

(a)

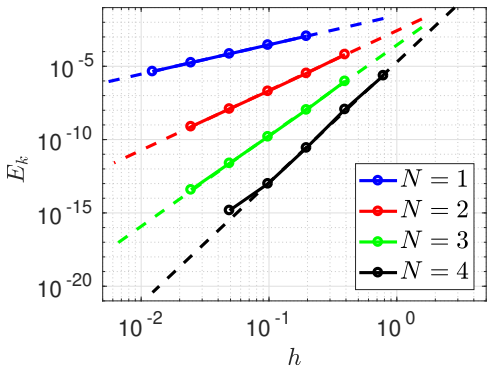

(b)

FIGURE 5. Relative errors e_k (a) and E_k (b) in Example 6.3 with $\lambda = 1$. The slopes of the dashed lines for e_k are 2.0 ($N = 1$), 3.0 ($N = 2$), 4.0 ($N = 3$) and 4.7 ($N = 4$), while those for E_k are 2.0 ($N = 1$), 4.0 ($N = 2$), 6.2 ($N = 3$) and 8.2 ($N = 4$).

[10] G. Emmanuele. Integrable solutions of a functional-integral equation. *J. Integral Equations Appl.*, 4(1):89–94, 1992.
[11] I. A. Ibrahim. On the existence of solutions of functional integral equation of Urysohn type. *Comput. Math. Appl.*, 57(10):1609–1614, 2009.
[12] X.-q. Jin, V.-K. Sin, and J.-y. Yuan. A wavelet method for the Fredholm integro-differential equations with convolution kernel. *J. Comput. Math.*, pages 435–440, 1999.
[13] F. Mirzaee and S. Piroozfar. Numerical solution of the linear two-dimensional Fredholm integral equations of the second kind via two-dimensional triangular orthogonal functions. *J. King Saud Univ. Sci.*, 22(4):185–193, 2010.
[14] N. Nahid, P. Das, and G. Nelakanti. Projection and multi projection methods for nonlinear integral equations on the half-line. *J. Comput. Appl. Math*, 359:119–144, 2019.
[15] S. P. Oliveira and J. S. Azevedo. Spectral element approximation of Fredholm integral eigenvalue problems. *J. Comput. Appl. Math.*, 257:46–56, 2014.
[16] S. P. Oliveira and J. S. Azevedo. Numerical approximation of 2D Fredholm integral eigenvalue problems by orthogonal wavelets. *Appl. Math. Comput.*, 267:517–528, 2015.

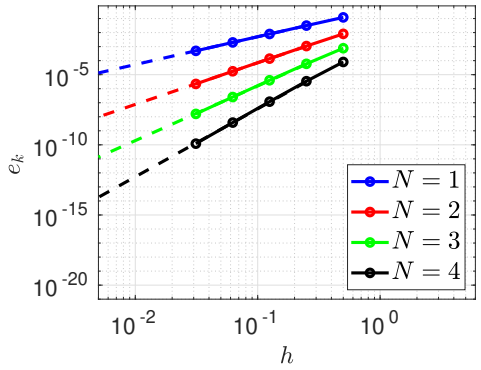

(a)

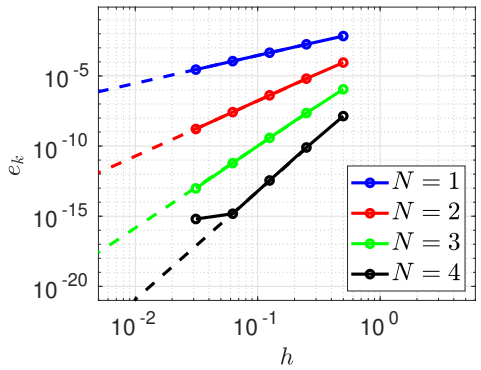

(b)

FIGURE 6. Relative errors e_k (a) and E_k (b) in Example 6.4. The slopes of the dashed lines for e_k are 2.0 ($N = 1$), 3.0 ($N = 2$), , 3.9 ($N = 3$) and 4.8 ($N = 4$), while those for E_k are 2.0 ($N = 1$), 3.9 ($N = 2$), 5.8 ($N = 3$) and 7.7 ($N = 4$).

[17] A. Patera. A spectral element method for fluid dynamics: Laminar flow in a channel expansion. *J. Comput. Phys.*, 54(3):468–488, 1984.

[18] S. Paul, M. M. Panja, and B. N. Mandal. Approximate solution of first kind singular integral equation with generalized kernel using Legendre multiwavelets. *Comput. Appl. Math.*, 38(1):23, 2019.

[19] A. C. Rocha, M. A. Murad, C. Moyne, S. P. Oliveira, and T. D. Le. A new methodology for computing ionic profiles and disjoining pressure in swelling porous media. *Computational Geosciences*, 20(5):975–996, 2016.

[20] A. M. Rocha, J. S. Azevedo, S. P. Oliveira, and M. R. Correa. Numerical analysis of a collocation method for functional integral equations. *Appl. Numer. Math.*, 134:31–45, 2018.

[21] A.-M. Wazwaz. *Linear and nonlinear integral equations*. Springer, Berlin, 2011.

[22] Y. Yang, Y. Chen, Y. Huang, and W. Yang. Convergence Analysis of Legendre-collocation methods for nonlinear Volterra type integro equations. *Adv. Appl. Math. Mech.*, 7(1):74–88, 2015.

[23] P. Zakian and N. Khaji. A stochastic spectral finite element method for wave propagation analyses with medium uncertainties. *Appl. Math. Model.*, 63:84–108, 2018.

Juarez S. Azevedo
ICTI-UFBA, Centro, 42809-000, Camaçari-BA, Brazil.
E-mail address: jdazevedo@ufba.br

Saulo P. Oliveira
DMAT-UFPR and INCT-GP, 81531-980, Curitiba-PR, Brazil.
E-mail address: saulopo@ufpr.br

Adson M. Rocha
CETEC-UFRB, Centro, 44380-000, Cruz das Almas-BA, Brazil.
E-mail address: adson@ufrb.edu.br